Stanisław FORTUNA*, Krzysztof SOBCZAK**

NUMERICAL AND EXPERIMENTAL INVESTIGATIONS OF THE FLOW IN THE RADIAL FAN

SUMMARY

The radial fan under investigation transfers energy in the form of mechanical work to the air. A three-dimensional flow structure in the rotor was determined on the basis of the computational and experimental data. A comparison of the numerical simulations by means of ANSYS CFX and thermoanemometer measurements of velocity as well as its components was presented. The results of numerical investigations, measurements and balance method were compared in order to determine the compressor performance characteristics.

Keywords*: fans, thermoanemometer measurements, numerical simulations, experimental characteristics*

BADANIA NUMERYCZNE I TERMOANEMOMETRYCZNO-BILANSOWE PRZEPŁYWU PRZEZ WENTYLATOR PROMIENIOWY

Wentylator przekazuje do czynnika energię w postaci pracy mechanicznej. Dla realnego wentylatora promieniowego wykonano numeryczną symulację przepływu za pomocą programu ANSYS, pomiary termoanemometryczne prędkości bezwzględnych i składowych za wirnikiem oraz pomiary bilansowe. Na podstawie uśrednionych profili odpowiednich prędkości wyznaczonych numerycznie i termoanemometrycznie wyznaczono parametry przepływowe wentylatora i porównano z eksperymentalną charakterystyką pracy wentylatora.

Słowa kluczowe*: wentylatory, pomiary termoanemometryczne, symulacje numeryczne, charakterystyki eksperymentalne*

NOMENCLATURE

V – volume flow
V_n – nominal flow rate
l_c – measured useful work (S–T)
l_u – theoretical calculated useful work in rotor
l_{kw} – energy losses in rotor inlet chamber
l_{ks} – energy losses in spiral chamber
l_{uc} – theoretical calculated useful work in fan (S–T)
D, b, β, a, b – geometrical parameters of fan (Fortuna 1999)
u – peripheral velocity

Indices:

$_1$ – rotor inlet
$_2$ – rotor outlet

1. INTRODUCTION

Four different methods were applied for the investigation of the air flow through the radial fan:

1. Experimental method, which is based on measurements of the fluid energy increment and the energy delivered to a fan drive at the test stand (Fortuna 2007). The experiments permit to determine the fan characteristics in conventional conditions of machine operation. These data are treated as reference for comparison of results obtained by means of other methods.
2. Analytical method, which is based on equations for the radial machine rotor.
3. Thermoanemometer measurements for determining the c_{2u} and c_{2r} velocity components.
4. Numerical simulations of the flow in a fan by means of ANSYS CFX code.

2. OBJECT OF INVESTIGATIONS

The fan section subjected to experimental and numerical investigations as well as the whole test stand (without fan volute) are presented in Figure 1. The fan under analysis works in a suction configuration.

The measurement cross-section is located in front of the rotor (OS). The data for fan characteristics were determined under specified conditions (density and nominal rpm) for a suction nozzle cross-section. The procedure of the characteristic determination is presented in (Fortuna 1999), while a characteristics required for the result comparisons are shown in Figure 5.

3. RADIAL MACHINE ROTOR CHARACTERISTICS

The formula of the work $l_{ut\infty}$ (as a function of the capacity $\dot{V} = 0.55\ \mathrm{m}^3/\mathrm{s}$) delivered to an ideal fluid in a fan rotor, which was determined under five assumptions (Fortuna 1999, 2005), is shown below:

$$l_{ut\infty} = u_2\left(u_2 - \frac{\dot{V}}{\pi\, D_2\, b_2\, \mathrm{tg}\beta_2}\right) = 1770.3\ \mathrm{m}^3/\mathrm{s} \qquad (1)$$

It is based on an linear approximation $l_{ut\infty} = C - \dot{V}B$ (see Fig. 2), where capacity $\dot{V}$ is an independent variable and constants are equal to: $B = u_2/(\pi\, D_2\, b_2\, \mathrm{tg}\beta_2)$ and $C = u_2^2$.

The capacity depends on geometrical and flow parameters at inlet nozzle (as in formula (2) or parameters at outlet nozzle:

$$\dot{V}_n = \pi\, D_1\, b_1\, u_1\, \mathrm{tg}\beta_1 = 0.252\ \mathrm{m}^3/\mathrm{s} \qquad (2)$$

* AGH University of Science and Technology in Krakow; s.fortuna1@wp.pl
** Institute of Turbomachinery, Technical University of Lodz; ksobczak@p.lodz.pl

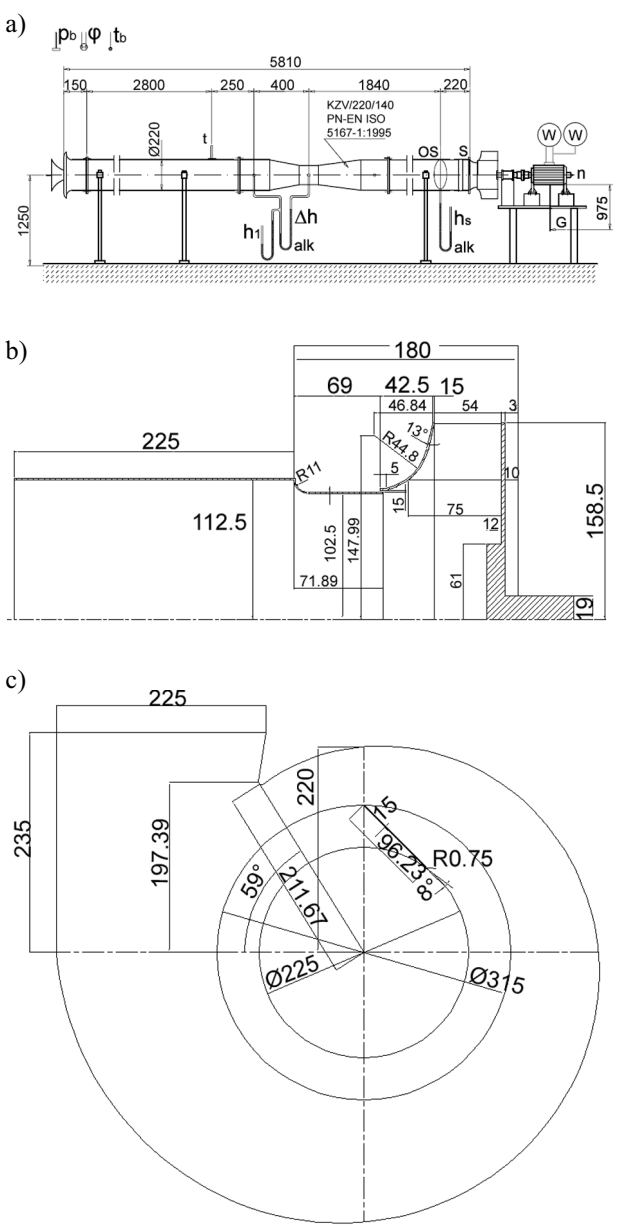

Fig. 1. Test stand configuration (a) and fan geometry (b, c)

Substituting the capacity (2) into formula (1) one can receive:

$$l_{ut\infty} = u_2^2 - u_2 u_1 T \quad \text{where} \quad T = \frac{D_1\ b_1\ \mathrm{tg}\beta_1}{D_2\ b_2\ \mathrm{tg}\beta_2} \tag{3}$$

Theoretical work l_{ut} is calculated by component method and after subtraction of $l_\mu = (1-\mu) l_{ut\infty}$, it can be represented by product: $l_{ut} = \mu l_{ut\infty}$, where

$$l_{ut} = \left(u_2^2 - u_2 u_1 T\right) - l_\mu = 1327\ \mathrm{m^2/s^2} \tag{4}$$

and useful work

$$l_u = l_{ut} - l_t - l_{nw} - l_v - l_b = 1115\ \mathrm{m^2/s^2} \tag{5}$$

The friction losses are determined from formula:

$$l_t = \xi_t \frac{w_{1a}^2}{2} \tag{6}$$

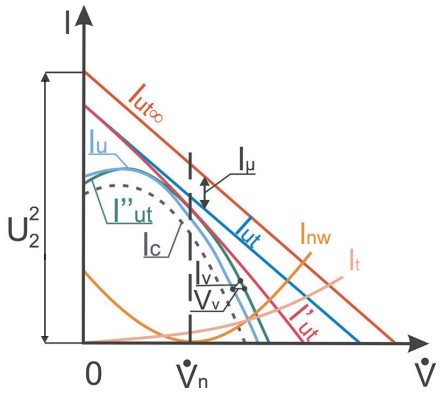

Fig. 2. Theoretical and conceptual characteristics of the fan l_u and experimental characteristics l_c

where:

$$w_{1a}^2 = \dot{V}_1^2 / \left(\pi\ D_1\ b_1\ \chi_1\ \sin\beta_1\right)^2,$$

$$\xi_t = (\lambda L)/d_{h1}, \lambda = 0.008 \cong 0,$$

$$d_{h1} = (2a_1 b_1)/(a_1 + b_1)$$

and finally:

$$l_t = \frac{\lambda L (a_1 + b_1)}{2a_1 b_1 \left(\pi\ D_1\ b_1\ \chi_1\ \sin\beta_1\right)^2} \dot{V}_1^2 = 32\ \mathrm{m^2/s^2} \tag{7}$$

Fanning losses:

$$l_b = \frac{K_b u_2^3 r_2^2}{2V} = 10\ \mathrm{m^2/s^2} \tag{8}$$

The incident losses (non-tangent inlet to the impeller):

$$l_{nw} = C u_2^2 \left(1 - V/\dot{V}_{1n}\right)^2 = 130\ \mathrm{m^2/s^2} \tag{9}$$

where:

$$C = 0.025,\ u_2 = \frac{\pi D_2 n}{60} = 47.5\ \mathrm{m/s},$$

$$u_2 = \frac{\pi D_2 n}{60} = 47.5\ \mathrm{m/s}$$

The volumetric losses are as follows:

$$l_v = \frac{V_v}{V} l_{ut} = 40\ \mathrm{m^2/s^2} \tag{10}$$

where:

$$V_v = \pi\ \mathrm{d_w}\ \mathrm{s}\ \alpha_v \sqrt{\Delta p_{ut}/\rho_1} = 0.016\ \mathrm{m^3/s},$$

$$\alpha_v = 0.57 \ \text{(Fortuna 1999)}.$$

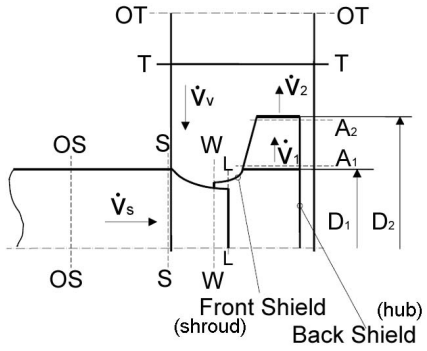

Fig. 3. Control sections in fan. Pressure measurements in sections OS and OT

Available work of fan can be determined between control sections T and S, as shown in Figure 3. However the flow losses between these sections have to be taken into account. As a result, the amount of work equals to:

$$l_{uc} = l_u - l_{kw} - l_{ks} = 1115 - 80 - 145 = 890 \text{ m}^2/\text{s}^2 \qquad (11)$$

where:
losses on the cone of inlet chamber and rotor according to formula

$$l_{kw} = \frac{1}{2}\xi_{kw} c_s^2 = 80 \text{ m}^2/\text{s}^2 \qquad (12)$$

losses in the volute

$$l_{ks} = 0.25\frac{c_3^2 - c_t^2}{2} = 145 \text{ m}^2/\text{s}^2 \qquad (13)$$

The calculated work points $l_{ut\infty}$, $l_{ut} = l_i$, and l_{uc} are shown in Figure 4.

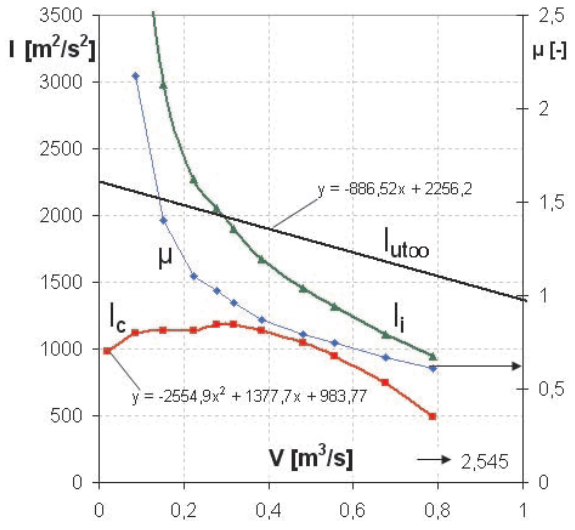

Fig. 4. Experimental characteristics l_c situated on the background of rotor work $l_{ut\infty}$, l_i, and μ

The detailed discussion of all loss components can be found in (Fortuna 2005a, b, c). The equation (5) allows to compare the work of machines determined by different methods. The results of the calculation by means of this method are shown in work (Fortuna 2006).

4. MEASUREMENT RESULTS

The available work was determined from formula (1) on the basis of the thermoanemometer measurements of radial and circumferential components of the velocity in absolute reference frame. Due to lack of the swirl at the rotor inlet the formula can be transformed into $l_u = u_2 c_{2u}$ and flow capacity $\dot{V}_s = \pi D_2 b_2 c_{2r}$. The measurements were carried in the volute along the line parallel to line T (Fig. 3), located 5–10 mm downstream of the rotor by means of triple-fibre thermoanemomether sensors. The averaged velocities along the rotor width are equal to $c_{2u} = 28.03$ m/s and $c_{2r} = 7.48$ m/s. It is equivalent to specific work $l_u = 1331$ m^2/s^2 and capacity $\dot{V}_{sp} = 0.40$ m^3/s. These parameters have to be recalculated at the control sections S-S and T-T. The losses in the rotor inlet chamber (91 m^2/s^2) and volute (95 m^2/s^2) can be determined on the basis of (Fortuna 2005a, b, c, 2006). Assuming the air density equals to 1.2 kg/m^3, the pressure rise in the fan is 1375 Pa. This point is marked on the fan characteristic (Fig. 5) with ⊗ sign. The fan characteristic curves presented in Figure 5 were obtained on the basis of the measurements of delivered energy by the fan drive unit. The results of velocity components c_{2u} and c_{2r} measurements are compared with numerical simulations results in the next chapter.

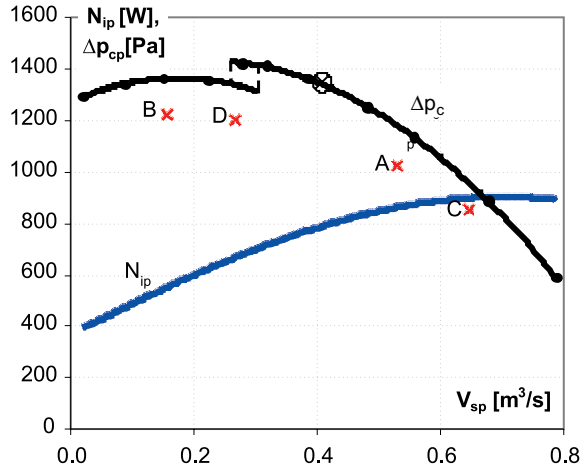

Fig. 5. Power and performance characteristics of the fan

5. NUMERICAL SIMULATIONS

The unsteady simulations of the air flow through the radial fan were conducted by means of ANSYS CFX code. The fan configuration with inlet pipe, rotor and volute are presented in Figure 6. The applied hexahedral mesh was composed of ~2 367 000 nodes. Application of authomatic mesh generators (ANSYS TurboGrid and ICEM Hexa) allowed to obtain good quality mesh grids presented in two cross-sections Figure 7.

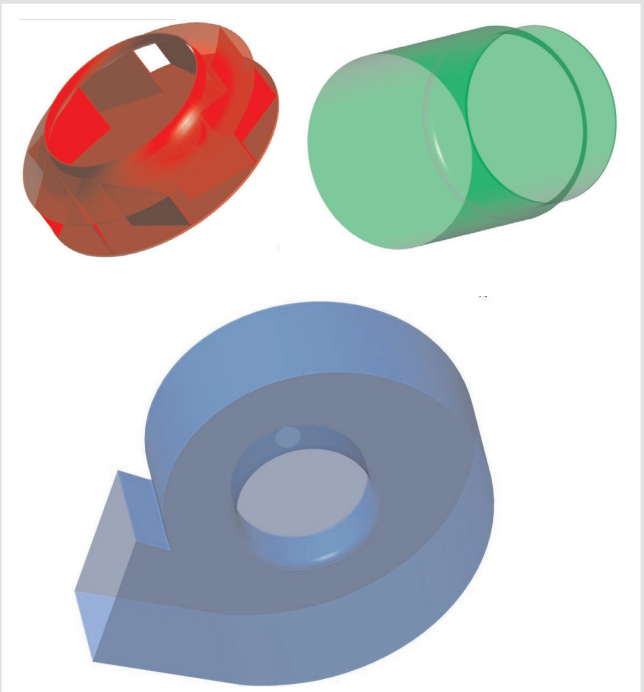

Fig. 6. Fan components

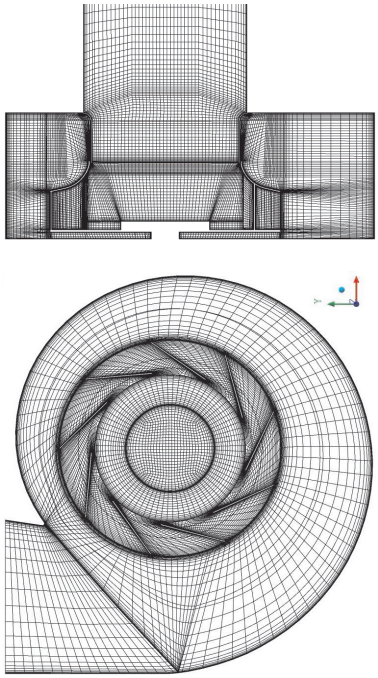

Fig. 7. Computational mesh

In the unsteady RANS simulations the SST turbulence model was applied with automatic wall function. The 3D N-S solution including boundary layers was not possible for such a complicated geometry due to available hardware limitations. The applied time step is equal to 1/90 of the impeller rotation period, i.e. 10 time steps per pitch. As a result, the Courant numbers reached the range 10–15. Its limitation to the optimal level (Co = 1) was not possible due to above-mentioned limitations. It can be expected that a part of the smallest unsteady phenomena may not be properly represented. Nevertheless, the resolved major structures mostly contribute to global parameter changes in the machine. A good level of the convergence was reached (RMS residuals did not exceed $1 \cdot 10^{-5}$) for the all time steps. The computations were carried out for 10 revolutions of rotor. The data for the analysis were derived after four initial revolutions. It was sufficient to obtain periodic behavior and convergence of the results.

The mass flow rate and temperature at the inlet of the fan as well as a static pressure at the outlet were imposed. These parameters were maintained constant in time. Details of the initial conditions are presented in Table 1. The fan impeller rotates 2880 rpm.

The values of the basic parameters obtained from numerical simulation are shown in the Table 2. Points A and C (see Fig. 5) are located stable part of the fan characteristic. In these cases, the pressure fluctuations in the fan have very low amplitudes. For points B and D, which are located on the unsteady part of the fan characteristics, the amplitudes of pressure variation are very high. These flow fluctuations are cased by the rotating stall. The typical characteristics of the pressure rise respect to the variations are shown in Figure 8.

Table 1. Initial conditions

	Point A	Point B	Point C	Point D
Mass flow rate at the inlet [kg/s] (corresponding flow rate [m^3/s])	0.636 (0.53)	0.1872 (0.156)	0.7764 (0.647)	0.3213 (0.267)
Static pressure at the outlet [Pa]	99935	99800	98300	98300
Air temperature at the outlet [K]	286.3	286.3	294.35	294.35
Turbulence intensity	≤ (1%)			

Table 2. Global calculation results

	Point A	Point B	Point C	Point D
Average of pressure rise [Pa]	1027	1226	854	1207
Pressure rise fluctuations [Pa]	45	500	60	475
Clearance flow [kg/s] (relative clearance flow)	~0.0364 (5.7%)	~0.0335 (17.9%)	~0.0362 (4.7%)	~0.0317 (9.9%)

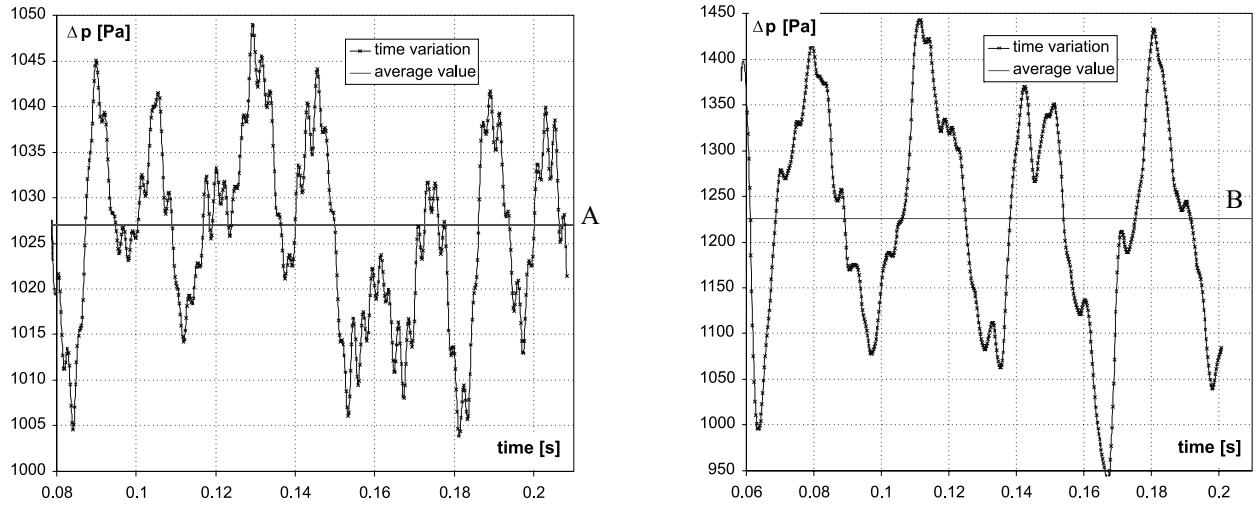

Fig. 8. Pressure rise variation for points A and B of the fan operation

The obtained data, marked by a red × sign in Figure 5, are compared with experimental measurement. Pressure rise in the fan obtained from numerical simulations is underestimated in all analysed cases. The differences are in the range of 100–150 Pa, however, the shape of the characteristic is properly preserved.

It can be noticed that the period of the fluctuations, in both cases presented in Figure 8, corresponds to approximately 1.5 of the rotor revolution. The mass flow rates through the inlet clearance between inlet pipe (funnel) and rotor shroud in all test cases are very similar. However, if the relative values are taken into account, the flows for points B and D (unsteady part of the fan characteristic) are considerable. In this point, it has to be stressed that gap is very small and the mesh in this region was relatively coarse, which affects the results. Nevertheless, it can be assumed the quantitative difference between points A/C and B/D is properly represented. In the area of unsteady fan operation the computations seem to be more sensitive to dynamic processes in comparison to manometer measurements with high dumping properties.

The distributions of the circumferential and radial velocity components along the blade height (from hub to shroud) 5 mm downstream the rotor are presented in Figure 9 for point A of the fan operation. Component distributions were obtained from circumferential averaging (360^o) of the results from the last time step of simulations. The significant increase of the circumferential component values are observed above 50% of the blade height. It is a result of the wake region growth at the trailing edge of the blades close to the shroud.

The computation results are compared with the hot-wire anemometer measurements described in the previous chapter. Unfortunately, the operation points in both approaches are different (see Fig. 5, ⊗ – measurements, × – computations), thus only qualitative comparisons are possible. The good qualitative agreement is observed for c_{2r} component. Significant discrepancies appear only in the hub vicinity. As far as c_{2u} component is concerned the significant differences in the hub region are shown, which spread up to 50% of the rotor blade height.

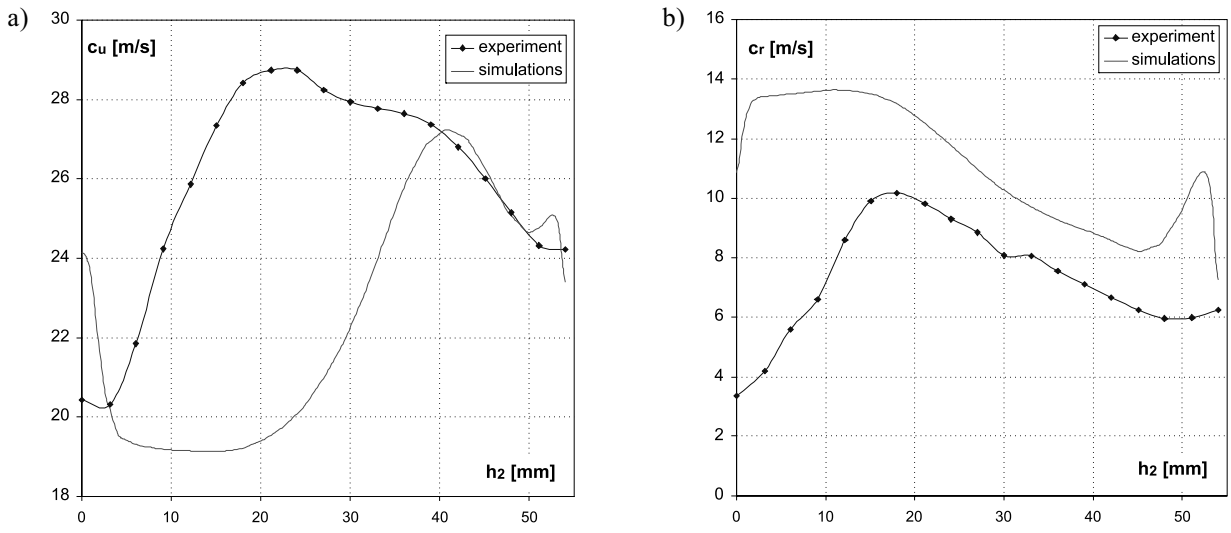

Fig. 9. Circumferential (a) and radial (b) velocity components 5 mm downstream the rotor

6. SUMMARY AND CONCLUSIONS

The low-pressure radial compressor (fan) was investigated. A comparison of the numerical simulations by means of ANSYS CFX and thermoanemometer measurements of velocity as well as its components was presented. Due to paper size limitations, the results based on an angular machine rotor equations are omitted.

Taking into account details of the fan geometry (e.g. gap between rotor shroud and inlet pipe (funnel), real shape of the rotor hub and shroud), complicated the mesh generation process. However, it led to the significant improvement in the prediction of the fan pressure rise as compared to simplified computations of the similar machine (Beczkowski *at al*. 2007). Nevertheless, some discrepancies still remain. In some cases these differences may be caused by the simplifications of the boundary conditions, based on the experimental results but without consideration for time and space variation of the parameters. The complexity flow structure (numerous unsteady separation zones) can be a source of errors resulting from limitations of the RANS method, particularly, limitations of the turbulence model with the wall function assumptions.

The comparison between the thermoanemometer measurements and CFD simulation clearly shows that properly conducted experimental investigations are still the most precise method of the machine performance determination. However, in the assumed range of the fan characteristics, the consistency of numerical simulations is satisfactory. Continuous progress in the CFD methods and computer capacities creates a great potential for a significant improvement of the simulation results quality in the foreseeable future.

References

Beczkowski J., Sobczak K., Borzęcki T., Jóźwik K. 2007, *Modelowe badania eksperymentalne i numeryczne promieniowego wentylatora energet.* VII Konferencja „Wentylatory i Pompy Przemysłowe", pp. 41–54 (in Polish).

Fortuna S. 1999, *Wentylatory*. Techwent, Kraków, pp. 131 (in Polish).

Fortuna S. 2005a, *Calculation of rotor work on the basis of thermoanemometric measurement results*. *Part 1.* Mechanics, vol. 24, No 1, pp. 8–14.

Fortuna S. 2005b, *Calculation of rotor work on the basis of thermoanemometric measurement results*. *Part 2*. Mechanics, vol. 24, No 1, pp. 14–20.

Fortuna S. 2005c, *Determination of loss coefficient in selected elements of radial fan*. Mechanics, vol. 24, No 4, pp. 234–239.

Fortuna S. 2006, *Experimental verification of theoretical work of rotor.* Mechanics, vol. 25, No 1, pp. 1–8.

Fortuna S. 2007, *Algorytm do wyznaczania dokładnych charakterystyk wentylatorów dla warunków umownych.* Ciepłownictwo, Ogrzewnictwo, Wentylacja, nr 11, pp. 16–18 (in Polish).